ACS Catalysis

Cite This: ACS Catal. 2018, 8, 4044−4048

Letter

pubs.acs.org/acscatalysis

Nanoceria-Supported Single-Atom Platinum Catalysts for Direct Methane Conversion

Pengfei Xie,[†] Tiancheng Pu,[†] Anmin Nie,[‡] Sooyeon Hwang,[#] Stephen C. Purdy,[∥] Wenjian Yu,[†] Dong Su,[#] Jeffrey T. Miller,[∥] and Chao Wang*[,†]

[†]Department of Chemical and Biomolecular Engineering, Johns Hopkins University, Baltimore, Maryland 21218, United States

[‡]Shanghai University Materials Genome Institute and Shanghai Materials Genome Institute, Shanghai University, Shanghai 200444, China

[∥]Davidson School of Chemical Engineering, Purdue University, West Lafayette, Indiana 47907, United States

[#]Center for Functional Nanomaterials, Brookhaven National Laboratory, Upton, New York 11973, United States

Supporting Information

ABSTRACT: Nanoceria-supported atomic Pt catalysts (denoted as $Pt_1@CeO_2$) have been synthesized and demonstrated with advanced catalytic performance for the nonoxidative, direct conversion of methane. These catalysts were synthesized by calcination of Pt-impregnated porous ceria nanoparticles at high temperature (ca. 1000 °C), with the atomic dispersion of Pt characterized by combining aberration-corrected high-angle annular dark-field scanning transmission electron microscopy (HAADF-STEM), X-ray photoelectron spectroscopy (XPS), X-ray absorption spectroscopy (XAS), and diffuse reflectance infrared Fourier transform spectroscopy (DRIFTS) analyses. The $Pt_1@CeO_2$ catalysts exhibited much superior catalytic performance to its nanoparticulated counterpart, achieving 14.4% of methane conversion at 975 °C and 74.6% selectivity toward C_2 products (ethane, ethylene, and acetylene). Comparative studies of the $Pt_1@CeO_2$ catalysts with different loadings as well as the nanoparticulated counterpart reveal the single-atom Pt to be the active sites for selective conversion of methane into C_2 hydrocarbons.

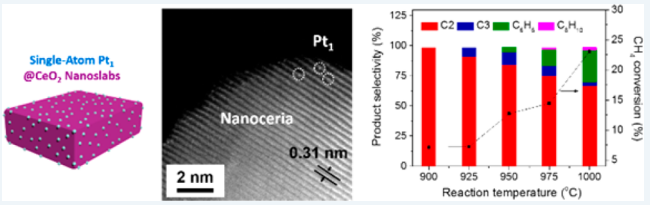

KEYWORDS: *single-atom catalysts, direct methane conversion, platinum, ceria nanocrystals, carbon coking*

INTRODUCTION

In recent years, natural gas has risen as a clean and cost-effective source of hydrocarbons, with great potential for replacing coal and crude oil in many sectors of energy and chemical industries.[1,2] The conventional approaches for methane conversion via syngas (a mixture of CO and H_2) is, however, challenged by the low carbon efficiency, large loss of exergy, and high capital cost associated with the complex, multistage processes.[3−5] Alternatively, direct conversion of methane can be achieved via oxidative coupling[6,7] or nonoxidative dehydrogenation[8−10] to produce olefins or aromatics. These approaches are believed to be more economical and environmentally friendly than via syngas.[11,12]

Single-atom catalysts (SACs) represent a new frontier of heterogeneous catalysis and have been extensively studied for many reactions, including CO oxidation,[13,14] water−gas shift,[15,16] methane steam reforming,[17] selective hydrogenation of alkynes and dienes,[18,19] and so on. The superior catalytic performance are usually attributed to the atomic dispersion of metal atoms with low coordination number, quantum confinement, and/or strong metal−support (mostly metal oxides) interactions.[20−22] It has also been reported that atomic Fe sites embedded in a silica matrix give rise to high catalytic selectivity for the nonoxidative conversion of methane to ethylene, aromatics, and hydrogen; the absence of metal ensembles suppresses C−C coupling and carbon coking, giving rise to long-term stability under the high-temperature reaction conditions.[10] Despite the progress, it remains elusive in many cases whether the single-atom sites offer distinct catalytic mechanisms from their ensembled counterparts with continuous surfaces.[21,22] One main obstacle is the lack of robust control over the dispersion of metals during the synthesis, and subnanometer clusters or nanoscale metal particles usually coexist with single metal atoms in the composite materials. The other challenge is the stability of the SACs under reaction conditions, especially considering the potential atomic aggregation and agglomeration at high temperatures.

Here we report the synthesis of ceria (CeO_2)-supported atomic Pt catalysts for direct conversion of methane into light hydrocarbons. Pt has been widely used to activate the C−H bond in hydrocarbons,[23−25] but carbon coking usually takes place on the conventional catalysts composed of Pt clusters or nanoparticles at high temperatures (e.g., > 800 °C), which has limited the application of Pt-based catalysts for methane

Received: January 1, 2018
Revised: February 26, 2018
Published: April 3, 2018

DOI: 10.1021/acscatal.8b00004
ACS Catal. 2018, 8, 4044−4048

conversion.[26,27] In this study, nanoceria-supported atomic Pt catalysts were synthesized by calcination of Pt-impregnated porous CeO_2 nanoparticles (Figure S1) at ca. 1000 °C (see the Supporting Information for experimental details). The obtained $Pt_1@CeO_2$ catalysts were characterized by using HAADF-STEM and XPS, and the absence of Pt ensembles was further confirmed by DRIFTS analysis using CO as a molecular probe. The $Pt_1@CeO_2$ catalysts of various loadings (with 0.5−1.0 wt % of Pt) were then evaluated for the methane conversion reaction, and the catalytic performance was further compared to their nanoparticulated counterpart to reveal the single-atom active sites.

RESULTS AND DISCUSSION

Figure 1a shows the representative transmission electron microscopy (TEM) image of the $Pt_1@CeO_2$ catalyst with

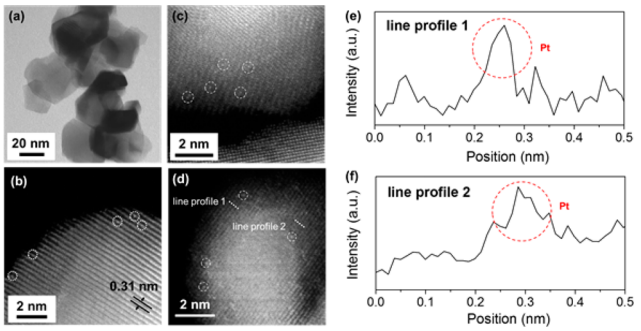

Figure 1. Representative (a) TEM and (b−d) high-resolution HAADF-STEM images of the $Pt_1@CeO_2$ catalyst with 0.5 wt % of Pt. (e,f) Intensity profiles of the scans along the dash lines marked in (d).

~0.5 wt % of Pt. They exhibit a slab-like morphology with the size varying from ~15 to ~40 nm, which were likely transformed from the porous nanospheres. High-resolution HAADF-STEM images reveal that Pt is dispersed on the CeO_2 nanoslabs at the atomic scale (Figures 1 b-d). In these images, individual Pt atoms are exhibited as bright dots with higher contrast than the surrounding CeO_2 lattice (Figures 1e,f). The slab-like nanocrystals exhibit lattice fringes with the spacing measured to be ca. 0.31 nm, which can be assigned to the (111) planes of CeO_2 in the fluorite phase (Figure 1b). Further synthesis shows that the ratio of Pt can be tuned from ca. 0.25−1.0 wt %, although Pt clusters start to appear in the 1.0% $Pt_1@CeO_2$ (Figure S2). For comparison, 3 nm Pt nanoparticles were also synthesized and deposited on similar CeO_2 nanoslabs (with 0.5 wt % of Pt, denoted as $PtNPs/CeO_2$) (Figures S3 and S4). X-ray diffraction (XRD) patterns collected for the $Pt_1@CeO_2$ catalyst only show the CeO_2 peaks in the fluorite ($Fm\bar{3}m$) phase (Figure S5), where the absence of Pt-phase peaks is consistent with the atomic dispersion of Pt as observed in the STEM images. The single-atom dispersion of Pt in the catalysts was further confirmed by CO chemisorption (Table S2) and extended X-ray absorption fine structure (EXAFS) analyses (Figure S8a). In particular, the EXAFS spectrum for 0.5% $Pt_1@CeO_2$ only exhibits one pronounced peak associated with the first-shell Pt−O bond (with Pt−O coordination number of 5 at ~2.03 Å), where the absence of Pt−Pt and higher-shell Pt−O−Pt scattering demonstrates atomic dispersion of Pt in the catalyst.

Oxidation state of Pt in the catalysts was characterized by using XPS (Figure 2). The spectrum collected for the 0.5%

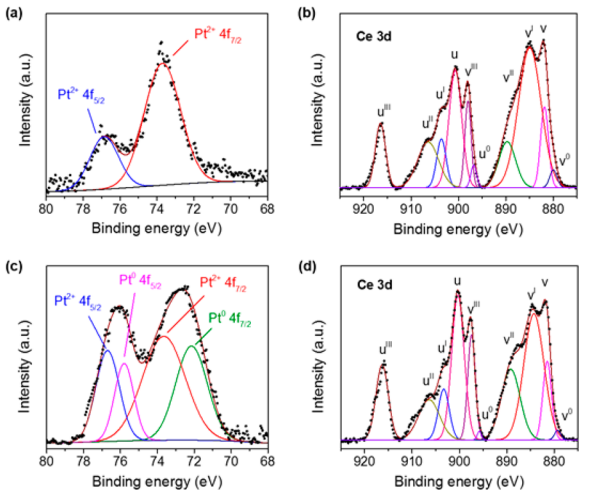

Figure 2. XPS spectra collected on the (a,b) 0.5% $Pt_1@CeO_2$ and (c,d) $PtNPs/CeO_2$ catalysts at the (a,c) Pt 4f and (b,d) Ce 3d edges.

$Pt_1@CeO_2$ catalyst shows two peaks at the Pt 4f edge with binding energies of 73.7 and 76.9 eV, which are assigned to the $4f_{7/2}$ and $4f_{5/2}$ states of Pt^{2+}, respectively (Figure 2a).[28,29] For $PtNPs/CeO_2$, the Pt 4f doublet exhibits downshift by ~1 eV in binding energy (Figure 2c). Deconvolution analysis reveals the presence of two additional peaks at 72.2 and 75.7 eV, in addition to the aforementioned two peaks associated with Pt^{2+}, which can be assigned to the same spin−orbital split of metallic Pt (Pt^0). The atomic ratio between Pt^{2+} and Pt^0 was estimated to be ~1.5 in the $PtNPs/CeO_2$ catalyst, with the oxidized Pt likely coming from surface oxidation of the Pt nanoparticles during calcination (see the Supporting Information for the details of synthesis).

The XPS spectra collected at the Ce 3d edge are shown in Figure 2b,d. The spectra can be deconvoluted on the basis of two multiplets that correspond to the $3d_{3/2}$ and $3d_{5/2}$ core holes of Ce (denoted as u and v, respectively) and have a spin−orbit splitting of ~18.6 eV:[30,31] u^0 (898 eV) and v^0 (880 eV) for $Ce(3d^94f^1)$-$O(2p^6)$, u (901 eV) and v (882 eV) for $Ce(3d^94f^2)$-$O(2p^4)$, u^I (904 eV) and v^I (885 eV) for $Ce(3d^94f^2)$-$O(2p^5)$, u^{II} (906 eV) and v^{II} (889 eV) for $Ce(3d^94f^1)$-$O(2p^5)$ and u^{III} (916 eV) and v^{III} (897 eV) for $Ce(3d^94f^0)$-$O(2p^6)$. The states marked with u^0/v^0 and u^I/v^I are features of Ce^{3+}, which was estimated to occupy ~46% and 33% of the Ce species in the 0.5% $Pt_1@CeO_2$ and $PtNPs/CeO_2$ catalysts, respectively (Table S1). These results indicate that the CeO_2 nanoslabs employed as support here are rich in Ce^{3+} defects and oxygen vacancies, which is likely a result of oxygen evolution during the high-temperature (1000 °C) treatment.

The XPS analysis shows that in the $Pt_1@CeO_2$ catalysts, Pt was dispersed on the CeO_2 support in the oxidized form (Pt^{2+}). It was reported that Pt can be emitted as volatile PtO_x above 800 °C in air.[14] The porous nanospheres (Figure S1) employed as precursor in the present study could have helped trap the PtO_x vapor, while Ce(III) and oxygen vacancies enriched on the formed CeO_2 nanoslabs represent coordinatively unsaturated, electrophilic sites and could have attracted and stabilized the atomic platinum oxides (e.g., in the form of planar $Pt^{2+}O_4$ clusters).[32] Thereby Pt was favorably dispersed as single-atom species in the derived $Pt_1@CeO_2$ catalysts.

DOI: 10.1021/acscatal.8b00004
ACS Catal. 2018, 8, 4044−4048

To gain a more extensive evaluation of the atomic dispersion of Pt, we have further performed diffuse reflectance infrared Fourier transform spectroscopy (DRIFTS) analysis of CO adsorption on the $Pt_1@CeO_2$ catalysts. This method has previously been demonstrated to be effective in identification of single Pt atoms on oxide supports.[13] Figure 3 compares the

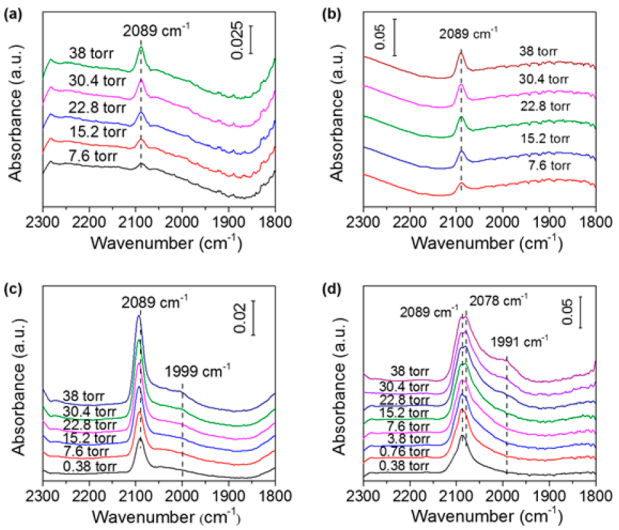

Figure 3. DRIFTS of CO chemisorption at different CO partial pressures on $Pt_1@CeO_2$ with various weight percentages of Pt: (a) 0.25%, (b) 0.5%, and (c) 1.0%. (d) $PtNPs/CeO_2$ (0.5 wt %) was also shown for comparison.

absorption spectra recorded on the $Pt_1@CeO_2$ catalysts with various loadings of Pt (0.25, 0.5, and 1.0 wt %) and $PtNPs/CeO_2$ (0.5 wt %), where CO was preadsorbed at different partial pressures. Only one peak was observed at 2089 cm^{-1} for the $Pt_1@CeO_2$ catalysts with 0.25% and 0.5% of Pt (Figures 3 a, b), which can be assigned to the linearly bonded CO (CO_L) on $Pt^{\delta+}$.[13] An additional peaks at 1991 cm^{-1} appears in 1.0% $Pt_1@CeO_2$ (Figure 3c), as well as $PtNPs/CeO_2$ (Figure 3d), which can be ascribed to the bridge bonded CO (CO_B) on Pt, a typical feature of Pt ensembles with continual surfaces.[13,33] $PtNPs/CeO_2$ exhibits another peak at 2078 cm^{-1} in addition to the two peaks observed on 1.0% $Pt_1@CeO_2$, which could be assigned to CO_L on the Pt nanoparticles with, for example, metallic Pt sites.[34] The absence of the CO_B peak thereby confirms the isolation of Pt sites in the $Pt_1@CeO_2$ catalysts at relatively low Pt ratios (e.g., < 1%), whereas Pt clusters have formed in the case with higher loadings.

After demonstrating the atomic dispersion of Pt, the $Pt_1@CeO_2$ catalysts were further evaluated for nonoxidative conversion of methane at 900−1000 °C with a space velocity of 6 L/(g_{cat}·h). Figure 4a summarizes the temperature-dependent methane conversion and product distribution for the 0.5% $Pt_1@CeO_2$ catalyst. The methane conversion increased with temperature and reached 23.1% at 1000 °C. The selectivity of C_2 hydrocarbons exhibited a gradual decrease from 98.4% at 900 °C to 66.7% at 1000 °C. The amount of C_3 product was rather small and always <10% throughout the investigated temperature range. At temperatures ≥950 °C, aromatic products started to appear and the selectivities increased with temperature, achieving 26.6% for benzene and 2.1% for naphthalene at 1000 °C. Breakdown of the C_2 product distributions is further elucidated in Figure 4b. At relatively low temperatures, ethylene and ethane were the two dominant

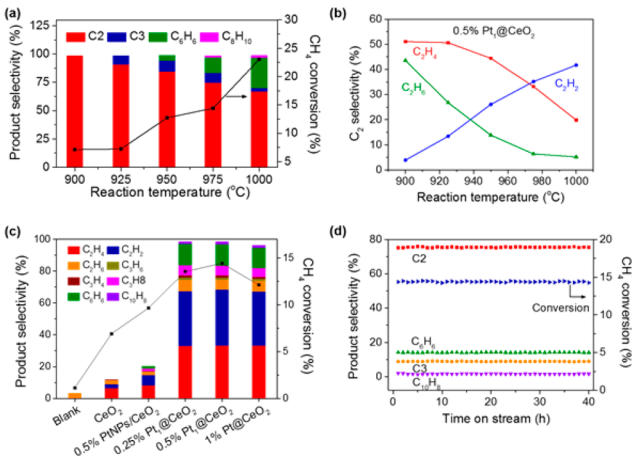

Figure 4. Catalytic performance for the nonoxidative CH_4 conversion evaluated at 6 L/(g_{cat}·h). (a) Catalytic activities and selectivities of the 0.5% $Pt_1@CeO_2$ catalyst as functions of the reaction temperature. Black squares represent CH_4 conversion and the colored histograms for product distributions. Here the light hydrocarbons are categorized as C_2 (ethane, ethylene, and acetylene) and C_3 (propane, propylene, and propyne) hydrocarbons, with further breakdown of the C_2 products shown in (b). (c) Comparison of methane conversion and product distributions at 975 °C over the different catalysts and the controls. (d) Stability test of the 0.5% $Pt_1@CeO_2$ catalyst performed at 975 °C.

products, with the selectivity measured to be 51.1% and 43.6% at 900 °C, respectively. At elevated temperatures, acetylene became more abundant and its selectivity achieved 41.7% at 1,000 °C, whereas only 19.8% of ethylene and 5.1% of ethane were left at this temperature. It is noticed that the amount of hydrogen generated from the methane conversion matches well with the concentrations calculated from the reaction stoichiometries and mass balance by taking the various hydrocarbon products into account (Figure S9).

The atomic Pt catalyst is far superior to its nanoparticulated counterpart for the methane conversion reaction. Figure 4c provides the comparison of methane conversion and product selectivity for the three $Pt_1@CeO_2$ catalysts with different Pt loadings as well as the $PtNPs@CeO_2$ catalysts at 975 °C (see the calculated turnover frequencies (TOFs) in Table S2). It is noted that even in the blank reaction tube, CH_4 had a conversion of 1.1% at this temperature due to the noncatalytic, thermal activation and dehydrogenation, but no hydrocarbons were detected in significant amounts (albeit with some ethane at 3.2% selectivity), suggesting that the converted methane mostly became coke (Figure S10) and deposited on the tube wall. The bare CeO_2 support exhibited somewhat higher (6.9%) CH_4 conversion, but coke was still the dominant (88.3%) product. The $PtNPs@CeO_2$ catalyst had a CH_4 conversion of 9.7%, with 8.3% and 6.3% selectivities toward ethylene and acetylene, respectively, whereas the majority (79.8%) of carbon also ended up as coke. All three atomic Pt catalysts performed much better than their nanoparticulated counterpart, achieving >12% conversion of methane and >95% of total selectivity toward hydrocarbons. Among the three $Pt_1@CeO_2$ catalysts, the 0.5% one demonstrates the highest conversion (14.4%) of methane and selectivity (74.3%) toward C_2 products, where ethylene (33.2%) and acetylene (35.1%) represent the major products. The slightly lower methane conversion and hydrocarbon selectivity from 1.0% $Pt_1@CeO_2$ can be ascribed to the presence of a small amount of Pt clusters

DOI: 10.1021/acscatal.8b00004
ACS Catal. 2018, 8, 4044−4048

in this catalyst, as can be seen from the STEM images (Figure S2) and DRIFTS analysis (Figure 3c).

The above observations clearly point to the single-atom Pt as active sites, which are not only able to activate the C−H bond by dehydrogenation, but also direct the C−C coupling toward favorable formation of C_2 hydrocarbons. In the cases of Pt nanoparticles and clusters, although the continuous metal surface is also activate for dehydrogenation, it lacks control over the extent of C−C coupling and cannot suppress the coking, which is consistent with the reported behavior of conventional catalysts with ensembles of metal atoms.[26,27,35] Besides suppression of carbon coking, the performance of the Pt_1@CeO_2 catalysts is noticeably different from the previously reported atomic Fe@SiO_2 catalysts, albeit with similar methane conversions (e.g., 12.7% for Pt_1@CeO_2 versus ∼8% for Fe@SiO_2 at 950 °C).[10] The single-atom Pt catalysts reported here give rise to much higher C_2 product selectivity than the Fe@SiO_2 (e.g., ∼84% versus ∼47% at 950 °C). In the latter case, the rest products are mainly aromatics (consistently at ∼50% independent of the reaction temperature) and nearly equally distributed between benzene and naphthalene. While the Pt_1@CeO_2 catalysts produce all the three kinds of C_2 species, ethylene is the only C_2 product obtained with the Fe@SiO_2 catalyst. These differences suggest that the Pt_1@CeO_2 catalysts may possess distinct catalytic mechanisms, particularly in the C−C coupling steps, from the Fe@SiO_2 catalyst, where multicarbon species were believed to form from gas-phase methyl ($^{\bullet}CH_3$) radicals via noncatalytic thermochemical processes.[10]

We have performed thermodynamic calculations for the equilibria of the involved conversion reactions toward different products (see the Supporting Information, section 3). The ratio of C_2 species in the product was found to be much higher than at equilibrium (Table S4). DRIFTS analysis of the Pt_1@CeO_2 catalyst after methane activation at 900 °C revealed the presence of π-bonded ethylene and acetylene, suggesting that the single Pt sites may be capable of stabilizing C_2 adsorbates (Figure S11). We thus propose that the methane conversion on the Pt_1@CeO_2 catalysts involves adsorbing C_2 intermediates, possibly formed from catalytic coupling of two dehydrogenated C_1 adsorbates (such as $*CH_3$ and $*CH_2$) on the single Pt sites (other than adjacent Pt sites as on the surface of Pt ensembles). As further coupling to form C_3 adsorbates may be inhibited on the atomically dispersed Pt, these C_2 intermediates must desorb and thus favor the production of C_2 hydrocarbons. The minor C_3 and aromatic products obtained at higher temperatures can be ascribed to the thermochemical dehydrogenation and oligomerization of the C_2 molecules in gas phase.

As discussed above, the primary role of the CeO_2 support in the Pt_1@CeO_2 catalysts is the stabilization of the single-atom Pt species, which could also be true under the reaction conditions.[32,36] However, synergetic effects may also be present between CeO_2 and Pt on the activation of CH_4. Active sites have been shown to be present at the interface between Pd clusters and CeO_2 with low methane activation barriers.[37] Although the situation may be different in the single-atom catalysts reported here, it should be noted that the onset temperature of methane activation on Pt_1@CeO_2 (i.e., ≤ 900 °C) is lower than that (≤950 °C) previously reported for single-atom Fe@SiO_2.[10] This is indicative of the active role of CeO2 in the methane conversion process other than only being an inert support.

Ultimately, we demonstrate that both the high catalytic activity and selectivity of the single-atom Pt_1@CeO_2 catalysts are stable, with indiscernible drop after 40 h of reaction at 975 °C (Figure 4d). The high durability further confirms the suppression of carbon coking on the active sites. The single-atom platinum-ceria catalysts reported here thus possess great potential for practical implementations.

■ ASSOCIATED CONTENT

Supporting Information

The Supporting Information is available free of charge on the ACS Publications website at DOI: 10.1021/acscatal.8b00004.

More experimental details, characterizations, and catalytic results (PDF)

■ AUTHOR INFORMATION

Corresponding Author

*E-mail: chaowang@jhu.edu.

ORCID

Dong Su: 0000-0002-1921-6683

Chao Wang: 0000-0001-7398-2090

Notes

The authors declare no competing financial interest.

■ ACKNOWLEDGMENTS

This work was supported by the IDEAS Program of the Advanced Research Projects Agency−Energy (ARPA-E), Department of Energy (DOE), and the Johns Hopkins Catalyst Award. Partial funding for S.C.P. and J.T.M. was provided as part of the National Science Foundation's Energy Resarch Center for Strategic Transformation of Alkane Resources (CISTAR) under Cooperative Agreement No. EEC-1647722. Electron microscopy work was performed at the Center for Functional Nanomaterials, Brookhaven National Laboratory, which is supported by the U.S. Department of Energy (DOE), Office of Basic Energy Science, under contract DE-SC0012704. Use of the Advanced Photon Source was supported by the U.S. Department of Energy, Office of Basic Energy Sciences, under contract No. DE-AC02-06CH11357. MRCAT operations are supported by the Department of Energy and the MRCAT member institutions.

■ REFERENCES

(1) Economides, M. J.; Wood, D. A. The state of natural gas. *J. Nat. Gas Sci. Eng.* **2009**, *1*, 1−13.

(2) McFarland, E. Unconventional Chemistry for Unconventional Natural Gas. *Science* **2012**, *338*, 340−342.

(3) Wood, D. A.; Nwaoha, C.; Towler, B. F. Gas-to-liquids (GTL): A review of an industry offering several routes for monetizing natural gas. *J. Nat. Gas Sci. Eng.* **2012**, *9*, 196−208.

(4) Torres Galvis, H. M.; Bitter, J. H.; Khare, C. B.; Ruitenbeek, M.; Dugulan, A. I.; de Jong, K. P. Supported Iron Nanoparticles as Catalysts for Sustainable Production of Lower Olefins. *Science* **2012**, *335*, 835−838.

(5) Saha, D.; Grappe, H. A.; Chakraborty, A.; Orkoulas, G. Postextraction Separation, On-Board Storage, and Catalytic Conversion of Methane in Natural Gas: A Review. *Chem. Rev.* **2016**, *116*, 11436−11499.

(6) Keller, G. E.; Bhasin, M. M. Synthesis Of Ethylene Via Oxidative Coupling Of Methane 0.1. Determination Of Active Catalysts. *J. Catal.* **1982**, *73*, 9−19.

(7) Zhu, Q. J.; Wegener, S. L.; Xie, C.; Uche, O.; Neurock, M.; Marks, T. J. Sulfur as a selective 'soft' oxidant for catalytic methane

DOI: 10.1021/acscatal.8b00004
ACS Catal. 2018, 8, 4044−4048

conversion probed by experiment and theory. *Nat. Chem.* **2013**, *5*, 104−109.
(8) Wang, L. S.; Tao, L. X.; Xie, M. S.; Xu, G. F.; Huang, J. S.; Xu, Y. D. Dehydrogenation And Aromatization Of Methane under Nonoxidizing Conditions. *Catal. Lett.* **1993**, *21*, 35−41.
(9) Morejudo, S. H.; Zanon, R.; Escolastico, S.; Yuste-Tirados, I.; Malerod-Fjeld, H.; Vestre, P. K.; Coors, W. G.; Martinez, A.; Norby, T.; Serra, J. M.; Kjolseth, C. Direct conversion of methane to aromatics in a catalytic co-ionic membrane reactor. *Science* **2016**, *353*, 563−566.
(10) Guo, X. G.; Fang, G. Z.; Li, G.; Ma, H.; Fan, H. J.; Yu, L.; Ma, C.; Wu, X.; Deng, D. H.; Wei, M. M.; Tan, D. L.; Si, R.; Zhang, S.; Li, J. Q.; Sun, L. T.; Tang, Z. C.; Pan, X. L.; Bao, X. H. Direct, Nonoxidative Conversion of Methane to Ethylene, Aromatics, and Hydrogen. *Science* **2014**, *344*, 616−619.
(11) Mesters, C. A Selection of Recent Advances in C1 Chemistry. *Annu. Rev. Chem. Biomol. Eng.* **2016**, *7*, 223−238.
(12) Schwach, P.; Pan, X. L.; Bao, X. H. Direct Conversion of Methane to Value-Added Chemicals over Heterogeneous Catalysts: Challenges and Prospects. *Chem. Rev.* **2017**, *117*, 8497−8520.
(13) Qiao, B. T.; Wang, A. Q.; Yang, X. F.; Allard, L. F.; Jiang, Z.; Cui, Y. T.; Liu, J. Y.; Li, J.; Zhang, T. Single-atom catalysis of CO oxidation using Pt_1/FeO_x. *Nat. Chem.* **2011**, *3*, 634−641.
(14) Jones, J.; Xiong, H. F.; Delariva, A. T.; Peterson, E. J.; Pham, H.; Challa, S. R.; Qi, G. S.; Oh, S.; Wiebenga, M. H.; Pereira Hernandez, X. I.; Wang, Y.; Datye, A. K. Thermally stable single-atom platinum-on-ceria catalysts via atom trapping. *Science* **2016**, *353*, 150−154.
(15) Yang, M.; Allard, L. F.; Flytzani-Stephanopoulos, M. Atomically Dispersed Au-$(OH)_x$ Species Bound on Titania Catalyze the Low-Temperature Water-Gas Shift Reaction. *J. Am. Chem. Soc.* **2013**, *135*, 3768−3771.
(16) Lin, J.; Wang, A. Q.; Qiao, B. T.; Liu, X. Y.; Yang, X. F.; Wang, X. D.; Liang, J. X.; Li, J. X.; Liu, J. Y.; Zhang, T. Remarkable Performance of Ir_1/FeO_x Single-Atom Catalyst in Water Gas Shift Reaction. *J. Am. Chem. Soc.* **2013**, *135*, 15314−15317.
(17) Duarte, R. B.; Krumeich, F.; van Bokhoven, J. A. Structure, Activity, and Stability of Atomically Dispersed Rh in Methane Steam Reforming. *ACS Catal.* **2014**, *4*, 1279−1286.
(18) Lucci, F. R.; Liu, J. L.; Marcinkowski, M. D.; Yang, M.; Allard, L. F.; Flytzani-Stephanopoulos, M.; Sykes, E. C. H. Selective hydrogenation of 1,3-butadiene on platinum-copper alloys at the single-atom limit. *Nat. Commun.* **2015**, *6*, 8550.
(19) Zhang, Z. L.; Zhu, Y. H.; Asakura, H.; Zhang, B.; Zhang, J. G.; Zhou, M. X.; Han, Y.; Tanaka, T.; Wang, A. Q.; Zhang, T.; Yan, N. Thermally stable single atom $Pt/m\text{-}Al_2O_3$ for selective hydrogenation and CO oxidation. *Nat. Commun.* **2017**, *8*, 16100.
(20) Yang, X. F.; Wang, A. Q.; Qiao, B. T.; Li, J.; Liu, J. Y.; Zhang, T. Single-Atom Catalysts: A New Frontier in Heterogeneous Catalysis. *Acc. Chem. Res.* **2013**, *46*, 1740−1748.
(21) Parkinson, G. S. Unravelling single atom catalysis: The surface science approach. *Chin. J. Catal.* **2017**, *38*, 1454−1459.
(22) Flytzani-Stephanopoulos, M. Supported metal catalysts at the single-atom limit - A viewpoint. *Chin. J. Catal.* **2017**, *38*, 1432−1442.
(23) Chin, Y. H.; Buda, C.; Neurock, M.; Iglesia, E. Reactivity of Chemisorbed Oxygen Atoms and Their Catalytic Consequences during CH4-O-2 Catalysis on Supported Pt Clusters. *J. Am. Chem. Soc.* **2011**, *133*, 15958−15978.
(24) Sattler, J. J. H. B.; Gonzalez-Jimenez, I. D.; Luo, L.; Stears, B. A.; Malek, A.; Barton, D. G.; Kilos, B. A.; Kaminsky, M. P.; Verhoeven, T. W. G. M.; Koers, E. J.; Baldus, M.; Weckhuysen, B. M. Platinum-Promoted Ga/Al_2O_3 as Highly Active, Selective, and Stable Catalyst for the Dehydrogenation of Propane. *Angew. Chem., Int. Ed.* **2014**, *53*, 9251−9256.
(25) Vajda, S.; Pellin, M. J.; Greeley, J. P.; Marshall, C. L.; Curtiss, L. A.; Ballentine, G. A.; Elam, J. W.; Catillon-Mucherie, S.; Redfern, P. C.; Mehmood, F.; Zapol, P. Subnanometre platinum clusters as highly active and selective catalysts for the oxidative dehydrogenation of propane. *Nat. Mater.* **2009**, *8*, 213−216.
(26) Kim, J.; Kim, W.; Seo, Y.; Kim, J. C.; Ryoo, R. n-Heptane hydroisomerization over Pt/MFI zeolite nanosheets: Effects of zeolite crystal thickness and platinum location. *J. Catal.* **2013**, *301*, 187−197.
(27) Zecevic, J.; van der Eerden, A. M. J.; Friedrich, H.; de Jongh, P. E.; de Jong, K. P. Heterogeneities of the Nanostructure of Platinum/Zeolite Y Catalysts Revealed by Electron Tomography. *ACS Nano* **2013**, *7*, 3698−3705.
(28) Matin, M. A.; Lee, E.; Kim, H.; Yoon, W. S.; Kwon, Y. U. Rational syntheses of core-shell Fe@(PtRu) nanoparticle electrocatalysts for the methanol oxidation reaction with complete suppression of CO-poisoning and highly enhanced activity. *J. Mater. Chem. A* **2015**, *3*, 17154−17164.
(29) Zhang, L.; Shen, Y. One-Pot Synthesis of Platinum-Ceria/Graphene Nanosheet as Advanced Electrocatalysts for Alcohol Oxidation. *ChemElectroChem* **2015**, *2*, 887−895.
(30) Lei, W. Y.; Zhang, T. T.; Gu, L.; Liu, P.; Rodriguez, J. A.; Liu, G.; Liu, M. H. Surface-Structure Sensitivity of CeO2 Nanocrystals in Photocatalysis and Enhancing the Reactivity with Nanogold. *ACS Catal.* **2015**, *5*, 4385−4393.
(31) Li, C. W.; Sun, Y.; Djerdj, I.; Voepel, P.; Sack, C. C.; Weller, T.; Ellinghaus, R.; Sann, J.; Guo, Y. L.; Smarsly, B. M.; Over, H. Shape-Controlled CeO2 Nanoparticles: Stability and Activity in the Catalyzed HCl Oxidation Reaction. *ACS Catal.* **2017**, *7*, 6453−6463.
(32) Dvorak, F.; Farnesi Camellone, M.; Tovt, A.; Tran, N. D.; Negreiros, F. R.; Vorokhta, M.; Skala, T.; Matolinova, I.; Myslivecek, J.; Matolin, V.; Fabris, S. Creating single-atom Pt-ceria catalysts by surface step decoration. *Nat. Commun.* **2016**, *7*, 10801.
(33) Aleksandrov, H. A.; Neyman, K. M.; Hadjiivanov, K. I.; Vayssilov, G. N. Can the state of platinum species be unambiguously determined by the stretching frequency of an adsorbed CO probe molecule? *Phys. Chem. Chem. Phys.* **2016**, *18*, 22108−22121.
(34) Moscu, A.; Schuurman, Y.; Veyre, L.; Thieuleux, C.; Meunier, F. Direct evidence by in situ IR CO monitoring of the formation and the surface segregation of a Pt-Sn alloy. *Chem. Commun.* **2014**, *50*, 8590−8592.
(35) Liu, L. C.; Diaz, U.; Arenal, R.; Agostini, G.; Concepcion, P.; Corma, A. Generation of subnanometric platinum with high stability during transformation of a 2D zeolite into 3D. *Nat. Mater.* **2017**, *16*, 132−138.
(36) Bruix, A.; Lykhach, Y.; Matolinova, I.; Neitzel, A.; Skala, T.; Tsud, N.; Vorokhta, M.; Stetsovych, V.; Sevcikova, K.; Myslivecek, J.; Fiala, R.; Vaclavu, M.; Prince, K. C.; Bruyere, S.; Potin, V.; Illas, F.; Matolin, V.; Libuda, J.; Neyman, K. M. Maximum Noble-Metal Efficiency in Catalytic Materials: Atomically Dispersed Surface Platinum. *Angew. Chem., Int. Ed.* **2014**, *53*, 10525−10530.
(37) Senftle, T. P.; van Duin, A. C. T.; Janik, M. J. Methane Activation at the Pd/CeO_2 Interface. *ACS Catal.* **2017**, *7*, 327−332.

DOI: 10.1021/acscatal.8b00004
ACS Catal. 2018, 8, 4044−4048